Fermi surface topology and de Hass-van Alphen orbits in $PuIn_3$ and $PuSn_3$ compounds

C.-C. Joseph Wang,[1] M. D. Jones,[2] and Jian-Xin Zhu[3]

[1] *Theoretical Division, Los Alamos National Laboratory, Los Alamos, New Mexico 87545, USA*
[2] *Department of Physics and Center for Computational Research, University at Buffalo-SUNY, Buffalo, New York 14260, USA*
[3] *Theoretical Division, Los Alamos National Laboratory, Los Alamos, NM 87545, USA*

(Dated: April 9, 2013)

Since the recent discovery of plutonium-based superconductors such as $PuCoIn_5$, systematic studies of the electronic properties for plutonium compounds are providing insight into the itinerancy-localization crossover of Pu $5f$ electrons. We are particularly interested in understanding the Fermi surface properties of $PuIn_3$ compound, which serves as the building block for the $PuCoIn_5$ superconductor. Motivated by the first observation of quantum oscillation and renewed interest in the de-Hass van-Alphen (dHvA) measurements on $PuIn_3$, we study the Fermi surface (FS) topology and the band dispersion in both paramagnetic and antiferromagnetic state of $PuIn_3$, based on density functional theory with generalized gradient approximation. We compare the results with its isostructural paramagnetic compound $PuSn_3$. We show the detailed Fermi surfaces of compounds $PuIn_3$ and $PuSn_3$ and conclude that the FS topology of an antiferromagnetic $PuIn_3$ agrees better with dHvA measurements. In addition, we show the magnetization of the antiferromagnetic order can alter the angle dependence and values of the effective mass for the dHvA orbits. We point out the accurate determination of the magnetic order orientation with respect to the crystal orientation is crucial to advance the understanding of the electronic structures of the $PuIn_3$ compound.

PACS numbers: 74.20.Mn, 71.27.+a, 74.70.Tx

I. INTRODUCTION

Actinide metals[1,2] are strongly correlated electronic systems due to the narrow bandwidth of $5f$ electrons. In addition, strong spin-orbit interaction within the $5f$ electron systems comparable to other energy scales renders the understanding of the electronic properties of the actinide metals more difficult. Itinerant-to-localized crossover of $5f$ electrons that occurs near plutonium in the actinide series is one of the most challenging issues in condensed matter physics, partly because the dual character (partially localized/delocalized) of these $5f$ electrons is closely related to the abrupt atomic volume variation between the α-Pu and δ-Pu metals. This change in bonding leads to a 25% larger volume in the δ phase as opposed to a low-symmetry, monoclinic crystal structure α phase of Pu, along with a variety of unusual physical and mechanical properties.[3] To understand the $5f$ electron delocalization-localization crossover in elemental actinide solids, it is very helpful to gain insight by studying its derivative compounds, which also show other emergent properties. One of the noticeable Pu-based compounds are 115 series. It has been discovered recently that superconductivity occurs in $PuCoGa_5$[4] ($T_c = 18.5$ K), $PuRhGa_5$[5] ($T_c = 8.7$ K), and $PuCoIn_5$[6] ($T_c = 2.5$ K) series. The detailed pairing mechanism in Pu-115 compounds are currently under intense investigation.[7] We are particularly interested in the electronic properties of $PuIn_3$ and its isostructural partner $PuSn_3$. The reasons are twofold. First, the $PuCoIn_5$ structure consists of stacked $CoIn_2$ and $PuIn_3$ layers, therefore the understanding of the electronic properties in $PuIn_3$ is relevant to uncovering the mystery of the superconductivity in $PuCoIn_5$. Second, the recent experimental capability to measure the Fermi surface topology of $PuIn_3$ by dHvA effects can help narrow down the minimal effective theory for these complicated systems.

In this paper, we present systematic studies of the electronic structures on $PuIn_3$ and $PuSn_3$ within density functional theory (DFT). We calculate the band dispersion, density of states (DOS), and the Fermi surface topology together with the identification of extreme orbits. For $PuIn_3$, there is recent experimental evidence[8] that the ground state of $PuIn_3$ is antiferromagnetic (AFM). However, the earlier dHvA measurement in this compound has been improperly interpreted in terms of DFT calculations based on a paramagnetic (PM) state of $PuIn_3$.[9] In the present work, we show the Fermi surface extreme orbits obtained for AFM $PuIn_3$ are in good agreement with the dHvA measurements, which places the theory and experiment comparison on a more consistent basis. Also with the known experimental fact of $PuSn_3$ being paramagnetic in the ground state, we predict a quite different band structure and Fermi surface topology in $PuSn_3$ as opposed to PM-$PuIn_3$. An experimental verification of this prediction will provide a significant support for Landau's Fermi liquid theory and demonstrate the potential toward the detection of quantum oscillations in δ-phase of Pu.

The organization of this paper is as follows. In Sec. II, we describe our theoretical method and briefly review the dHvA effects in itinerant electronic systems like metals. In Sec. III A, we discuss the band structures of the $PuIn_3$ and $PuSn_3$ compounds, respectively. In Sec. III B, DOS for the two compounds in concert to the band structures are discussed. In Sec. III C, we show the Fermi surface

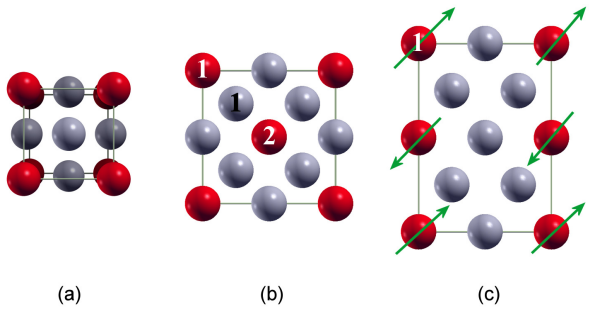

FIG. 1: (Color online) (a) PM-PuM$_3$(M=In,Sn) conventional unit cell. Red sphere: Pu, Grey sphere: M; (b) Top view of the anti-ferromagnetic PuIn$_3$ conventional unit cell; (c) Side view of the anti-ferromagnetic PuIn$_3$ conventional unit cell. The green arrows illustrates the commensurate AFM order. The tilt arrow just indicates the spontaneous symmetry breaking orientation for viewing convenience. The actual orientation for our studies can vary.

topology and the corresponding dHvA orbits, which are relevant to available experimental studies. Discussions and conclusions are summarized in section IV.

II. THEORETICAL METHOD

PuIn$_3$ and PuSn$_3$ compounds crystallize into cubic AuCu$_3$-type structure at room temperature and have the actinide-actinide distance far above the Hill limit,[10] making the $5f$-ligand hybridization the dominant mechanism for Pu $5f$-electron delocalization. The lattice constants are given by 4.61$\mathring{A}$ for PuIn$_3$,[11] and 4.63$\mathring{A}$ for PuSn$_3$,[12] respectively. PuSn$_3$ was reported as a paramagnet experimentally.[13] However, the PuIn$_3$ was originally assumed[9] to be also paramagnetic but more recent experiments indicate it is in an AFM state below 14 K.[8] In this work, we consider both PM and AFM cases for the PuIn$_3$ compound. The conventional unit cell of PM-PuM$_3$ (M=In, Sn) is shown in Fig. 1(a) with the ligand atoms M situated at face centers of the cell. The magnetic unit cell for the AFM-PuIn$_3$ is enlarged because it is the commensurate AFM order obeying the discrete translational invariance in the crystal. Figure 1(b) shows the top view of the magnetic unit cell accommodating the commensurate AFM order. The side view is shown in Fig. 1(c). Therefore, the lattices in this case can be considered as a tetragonal Bravais lattice decorated with the basis with Pu and In atoms.

The first-principles calculations used here are based on the generalized gradient approximation with the PBE (96) functional.[14] We use the scheme of the full-potential linear augmented plane wave basis plus local basis[15] (FP-LAPW+lo), as implemented in the WIEN2K code.[16] The LAPW sphere radii R used for Pu, In, Sn atoms are 2.5 Bohr. The interstitial plane wavenumber cut-off $k_{max}R = 8.0$ is chosen for the basis set. The semi-core states (Pu $6s6p$, In $4p$) are included with the valence electrons using local orbitals. The core states are treated at the fully relativistic level with spin-orbital interaction for all atoms. The spin-orbital interaction for semi-core and valence states are incorporated by a second variational procedure[17] using the scalar relativistic eigenstates as basis, except that the so-called $6p_{1/2}$ relativistic local orbitals[18] are used to account for the finite character of the wave function at the Pu nucleus. Dense Brillouin zone sampling is used for the calculation of the Fermi surface. We use a 31 $\times$ 31 $\times$ 31 k-mesh for the PM-PuIn$_3$ and PuSn$_3$ calculations. A 31$\times$ 31 $\times$ 22 k-mesh is used for the AFM PuIn$_3$. Experimentally, a full determination of the magnetic structure for the AFM state of PuIn$_3$ is currently not available. Therefore, we assume this structure follows that of its isostructural compound: CeIn$_3$.[19,20] This choice is also supported by Fermi surface topology of PM-PuIn$_3$ as discussed later. The dHvA effect is observable in very clean metallic systems, typically in strong magnetic fields exceeding several tesla. On sweeping the magnetic field $\mathbf{B}$, one observes oscillations in the magnetization, which are periodic in an inverse magnetic field due to the fact that the number of occupied Landau levels changes with the magnetic field. The measurement of dHvA effect with varying magnetic field orientation is a powerful probe on Fermi surface topology in metallic and inter-metallic systems. The dHvA frequency F in MKS units is related to the extremal Fermi surface cross-sectional area A surrounded by extremal cyclotron orbits perpendicular to the magnetic field orientation:[21]

$$F = \frac{\hbar}{2\pi e} A \tag{1}$$

where e is the elementary charge. In addition, the effective mass of electrons averaged around the cyclotron orbits can be determined by the damping strength of dHvA measurements as a function of temperature. Our determination of the dHvA orbits is based on the numerical algorithm implemented by Rourke and Julian.[22]

III. RESULTS

A. Band structures

Since PM-PuM$_3$ compounds can be generated from the cubic unit cell in space, the corresponding BZ is cubic in reciprocal space. For simplicity, we label high-symmetry $\mathbf{k}$ points by the notation adopted by the tetragonal unit cell, as shown in Fig. 2, even though the BZ for the PM-PuM$_3$ is cubic.

The band structure for both PM-PuIn$_3$ and PuSn$_3$ demonstrates two bands across the Fermi energy. The energy dispersion along the high symmetry points is shown in Figs. 3 and 4. We observe the Fermi energy is crossed by two bands mainly of $5f$ electron character, as shown later in the density of states (DOS) studies. The f-bands are far from flat due to the hybridization mainly from

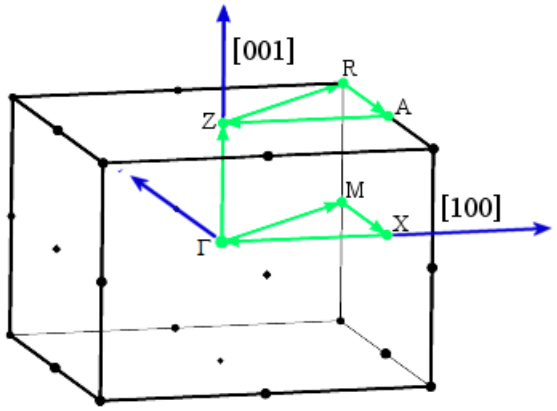

FIG. 2: (Color online) Tetragonal Brillouin zone (BZ). The symmetry points are labeled by capital letters.

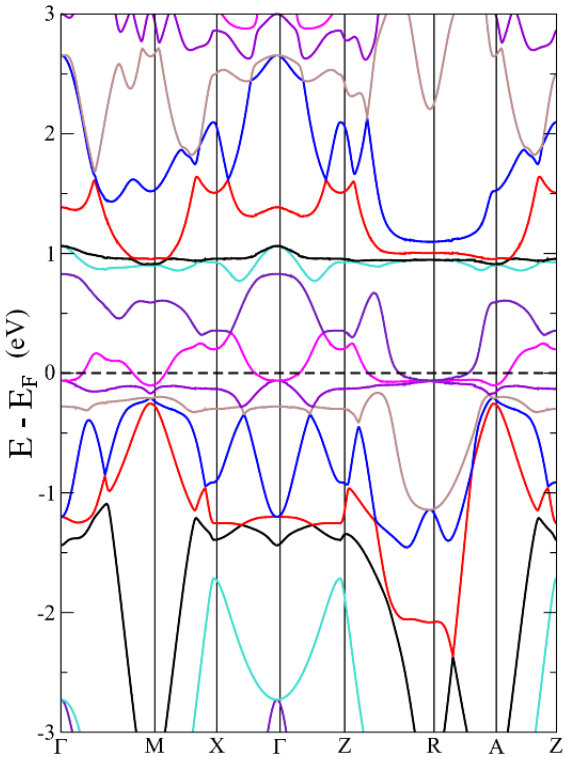

FIG. 3: (Color online) Band structure of the PM-$PuIn_3$ along the high symmetric points in BZ.

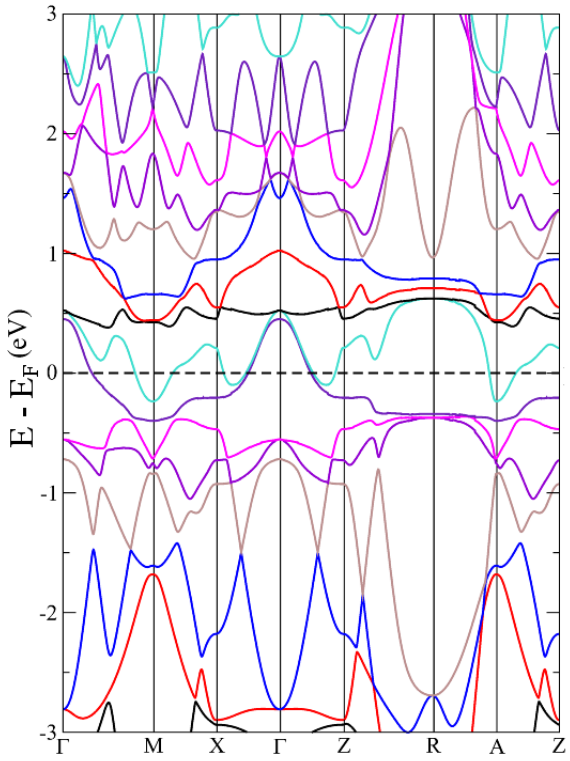

FIG. 4: (Color online) Band structure of the PM-$PuSn_3$ along the high symmetric points in cubic BZ. Two conduction bands are across the Fermi level E_F.

the $5p$ valence electron of ligand atoms. We calculate the band structure of PM-$PuIn_3$ and PM-$PuSn_3$ by the density functional theory using the GGA approximation. We notice that the energy dispersion for PM-$PuSn_3$ is very different, which indicates that the PM-$PuIn_3$ and PM-$PuSn_3$ have very different Fermi surface topology, which is discussed in Sec. III C.

For the AFM $PuIn_3$ with the chosen magnetic unit cell, the BZ in the reciprocal lattices becomes tetragonal. Let us first discuss the circumstances in which magnetic moment orientation $\boldsymbol{\sigma}$ for the AFM order is parallel to [001] direction defined by PM-$PuIn_3$ crystal unit cell. There are more atoms in the unit cell and therefore far more bands are accommodated in the corresponding tetragonal BZ. We observe four bands crossing the Fermi energy E_f as shown in Fig. 5. In this case, the bandwidth of $5f$ bands across Fermi surface is much narrower than the bandwidth in the PM case. The energy bands near the Fermi energy have dominant $5f$ electron features, as shown later in the DOS, and have large effective band mass because of the flatness of the bands.

B. Density of states

By the smaller equilibrium volume of $PuIn_3$ in comparison with $PuSn_3$, one may argue that PM-$PuIn_3$ should

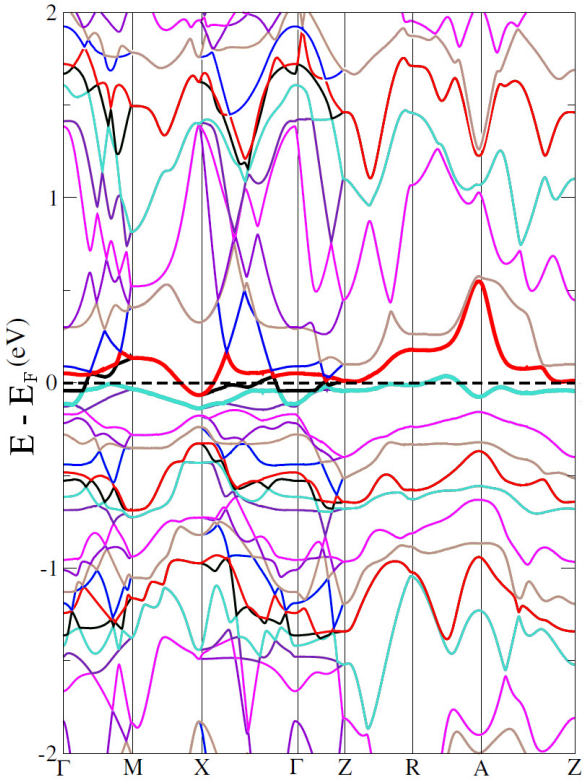

FIG. 5: (Color online) Band structure of the AFM-$PuIn_3$ along the high symmetric points in tetragonal BZ with the local spin polarization $\boldsymbol{\sigma} \parallel [001]$.

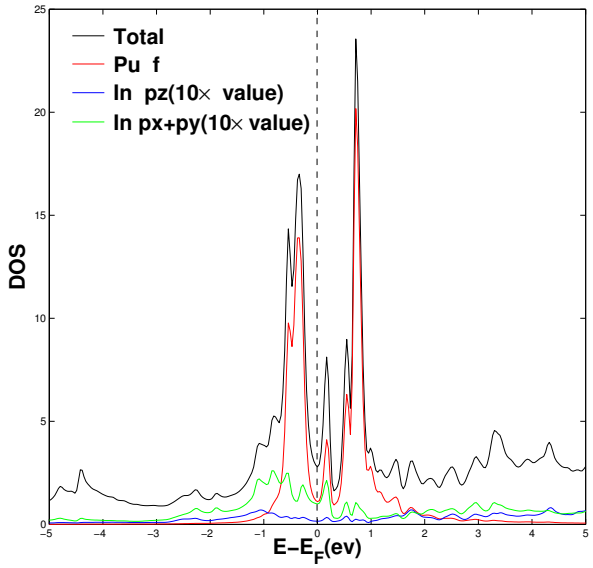

FIG. 6: (Color online) DOS per atom and total DOS in PM-$PuIn_3$ compound. Ten times of the actual density of states for p orbitals at In site are plotted for better contrast. The black solid line shows the total DOS in the BZ.

have a more itinerant $5f$ bands in comparison with $PuSn_3$ due to the smaller distance between nearest-neighboring Pu atoms and the In atoms. In addition, the atomic $5p$ levels from ligand atoms in $PuIn_3$ tend to be more delocalized due to smaller attraction from nucleon charges. However, those effects are not expected to be very remarkable in the DOS because of the closeness of the atomic properties for the In atom and Sn atom.

To understand the hybridization between Pu $5f$ and ligand valence states, we perform the DOS calculation for these compounds. In Fig. 6, the DOS for the PM-$PuIn_3$ is shown. We observe a nonzero total DOS near the Fermi level. The peak near the Fermi energy shows a hybridization of Pu $5f$ with the DOS of $5p$ valence electrons from the In atom. This indicates that the metallic behavior is inherent from the hybridization of $5f$ localized electrons at Pu with $5p$ itinerant electrons at In. The two strong peaks away from the Fermi surface are due to the strong spin-orbital coupling for the localized f electrons, which is weakly hybridized with In $5p$ orbitals. The lower peak is mainly due to $j = 5/2$ sub-bands and the higher peak is mainly due to $j = 7/2$ sub-bands, which has been studied previously by relativistic Stoner theory.[23] The $5f$ electron occupancy at Pu atomic sphere is around 4.8. This suggests that the mid-peak near Fermi energy originates from the higher $j = 5/2$ sub-bands in the presence of crystal-field splitting. The three-peak features are similar also in $PuSn_3$ except the $j = 5/2$ peak are broadened by the hybridization from Sn p orbitals. Fig. 7 presents the DOS for $PuSn_3$. We notice the $j = 5/2$ sub-bands are still sharply peaked but with a slightly larger $5f$-DOS at Pu site as shown by the solid-red line as suggested by a slightly smaller hybridization. As will be mentioned later, PM-$PuIn_3$ and PM-$PuSn_3$ have very different Fermi surface topology despite of the similarity in DOS.

We have also calculated the DOS for the AFM-$PuIn_3$, as shown in Figs. 1(b) and 1(c), the lattice can be divided into two sub-lattices. The calculated spin projected partial DOS at different atomic sites is shown in Fig. 8. We observe that the Pu1 atom has larger $5f$ occupancy in the up-spin channel (see corresponding partial DOS as denoted by "blue" solid line). However, the Pu2 atom takes larger $5f$ occupancy in the down-spin channel (see corresponding partial DOS as denoted by "blue" dotted line). This indicates that Pu1 and Pu2 atoms have magnetic moments due to $5f$ electrons, which are equal in magnitude but antiparallel in orientation. We do not observe net magnetic moment at In atoms according to the equal spin-projected DOS for the In1 atom indicated by the solid-dashed curves. The AFM order has the effect of generating a gap, above the Fermi energy, between two major peaks belonging to up and down spin Pu $5f$-DOS. By our first-principle calculation, we found the orbital moment at Pu1 atom is around $-2.1\mu_B$ (μ_B : Bohr magneton) but changes sign (-2.1μ_B) for Pu2 atom. The spin

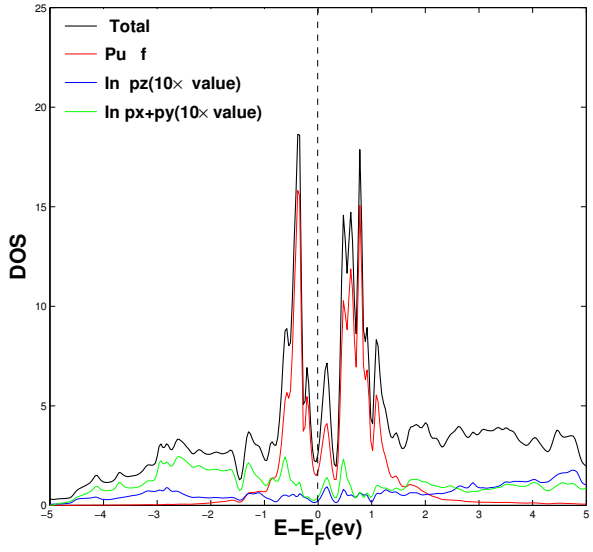

FIG. 7: (Color online) DOS per atom and total DOS in a PM-$PuSn_3$ compound. Ten times of the actual DOS for p orbitals at Sn site are plotted for better contrast. The black solid line shows the total DOS in the BZ.

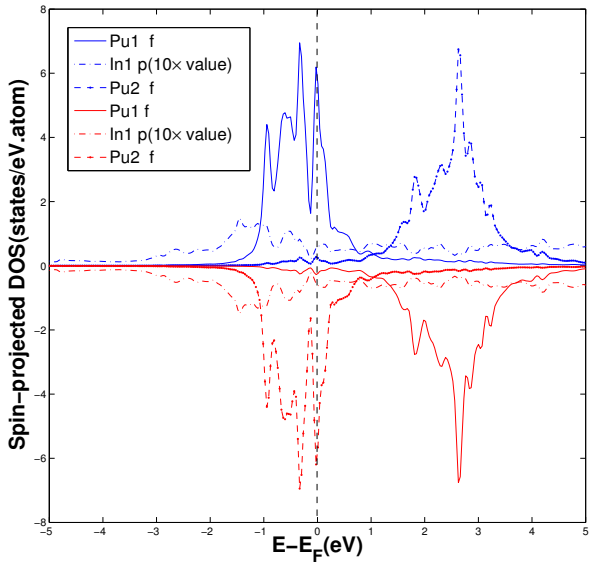

FIG. 8: (Color online) Spin-projected DOS for the AFM-$PuIn_3$ compound. Pu1 represents the Pu atom with a positive local magnetic moment. Pu2 represents the Pu atom with a negative local magnetic moment. It is noted that Pu1 atom and Pu2 atom are the nearest neighbors in the AFM unit cell. The In1 atom indicates the indium atom located between the Pu1 and Pu2 atom in the unit cell (Figs. 1(b) and 1(c)). The color "blue" indicates the up-spin projected DOS along the chosen quantization $+z$ axis in Bloch sphere. The color "red" indicates the down-spin projected DOS along the $-z$ axis in Bloch sphere. Ten times of the actual spin-projected DOS of p orbitals at the In1 site are plotted for better contrast.

moment at Pu1 and Pu2 atoms are given by $4.7\mu_B$ and $-4.7\mu_B$ respectively. We observe the presence of magnetic order causes the mixing of $j = 5/2$ and $j = 7/2$ and turn the local dip structure near the Fermi surface to a peak structure. In addition, two major peaks in DOS appear away from Fermi surface with large energy separation between maxima.

C. Fermi surface topology and dHvA orbits

In this section, we show the Fermi surface topology and calculate the dHvA frequencies as a function of magnetic field orientation for compounds $PuSn_3$ and $PuIn_3$. By the band structure calculation, Fermi surface topology is determined by the isosurface calculated by the eigenstates of Kohn-Sham equation.

PM-$PuIn_3$ compound

The Fermi surfaces for PM-$PuIn_3$ from two conduction bands are shown in Figs. 9 and 10. The ordering of bands are based on the energies in increasing order in the band dispersion (Fig. 3). There are two bands across the Fermi level. The characters of the dHvA orbits are tabulated in Tables I and II respectively. We present the dHvA orbits of interest by "yellow" orbits or the label "orbit 1" for later discussion. This is highlighted in the final two columns in Tables I and II. For Band-1, when the magnetic field is chosen along [111] direction, four dHvA orbits are identified in the BZ as listed in Table I. Three of the orbits are electron-like and one is hole-like. The dHvA orbit labeled by 1 originates from the Fermi surface near the center of BZ and has the dHvA frequency $F = 0.9627$ kiloTesla(kT). The location of the orbit 1 is shown in Fig. 9 explicitly. The other orbits with much larger dHvA frequencies are not our main focus since the dHvA frequencies are far from what have been observed experimentally.[9] For Band-2, only an electron-like (yellow) orbit with the dHvA frequency $F = 3.9206$ kT near the corner of the BZ is found, which is shown in Fig. 10. As far as the field angular dependence is concerned, we focus on the orbits which are connected with the same Fermi surface surrounded by the yellow orbits from Band-1 and Band-2 at the field orientation [111]. We observe the continuation of the orbits from the same Fermi surface spanned the whole angle range from [100] to [111] field orientation. In addition, the calculated dHvA frequencies are not close to 2 kT as shown in Fig. 11(a). Those facts contradict the observed dHvA frequency (around 2 kT) which only survives a limited span of field angles.[9] This indicates that the assumption of the PM state in $PuIn_3$ is problematic for the interpretation of the electronic properties of the $PuIn_3$ compound.

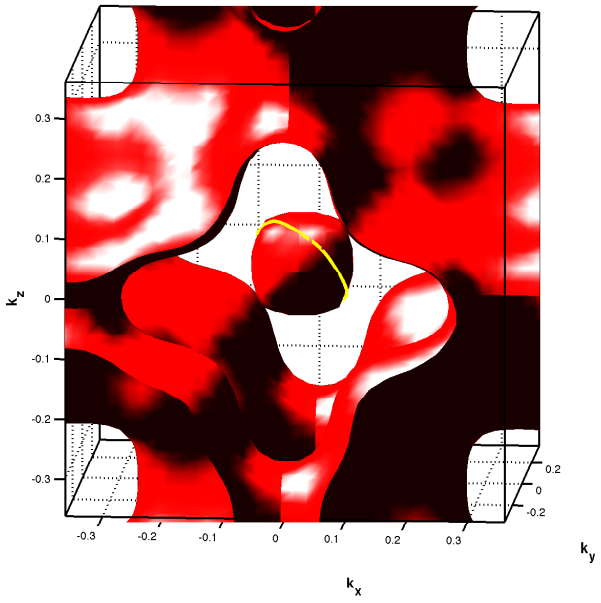

FIG. 9: (Color online) Fermi surface from Band-1 in PM-$PuIn_3$ compound.

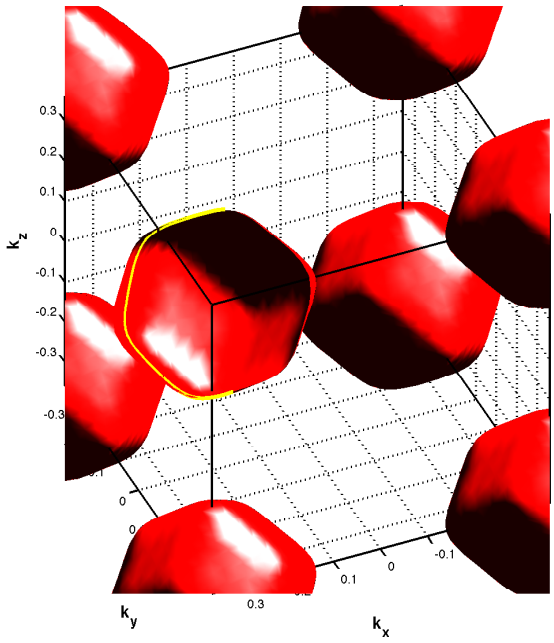

FIG. 10: (Color online) Fermi surface from Band-2 in PM-$PuIn_3$ compound.

From the Fermi surface topology for PM-PuIn3 in Figs. 9 and 10, we notice the nesting between the small Fermi surface at the Γ point from Band-1 and the four Fermi surfaces at the corners of BZ from Band-2. The nesting wave vector between the Fermi surfaces is approximately $(\pi/a, \pi/a, \pi/a)$. Therefore, magnetic instability for commensurate AFM order should indeed be favored. In the following, we study commensurate AFM order in $PuIn_3$.

TABLE I: dHvA orbits from Band-1: PM-$PuIn_3$, **B** ∥ [111]

F(kT)	$m^*(m_e)$	Type	Number	Color	Label
16.149	6.4320	h	1	–	–
13.209	4.9218	e	1	–	–
10.818	6.02	e	2	–	–
0.9627	2.4587	e	1	–	1

TABLE II: The dHvA orbit from Band-2: PM-$PuIn_3$, **B** ∥ [111]

F(kT)	$m^*(m_e)$	Type	Number of orbits	Color	Label
3.9206	3.3774	e	1	yellow	1

AFM-$PuIn_3$ compound

From the band structure calculations as shown earlier in Fig. 5, there are 4 bands across the Fermi level for AFM $PuIn_3$. The labeling of bands still follow the band energies (Band-1, Band-2, etc.). The corresponding Fermi surfaces and dHvA orbits (when the external magnetic field is orientated along [111] direction) are illustrated in Figs. 12-15, respectively. We are interested in dHvA orbits with dHvA frequencies around 2 kT, which are labeled as orbit 1 for Band-2 and Band-3 in Tables IV and V. The information of other dHvA orbits due to Band-1 and Band-4 are listed in Tables III and VI. We provide the Fermi surface topology for Band-1 and Band-4 in Figs. 12 and 15 for reference.

For Band-2, the yellow orbits with the dHvA frequency of 1.3908 kT around the Fermi surface at the corner of the BZ are illustrated in Fig. 13. When the field orientation varies, one expect dHvA orbits at different angle are continued orbits from the same Fermi surface. Therefore, we expect the dHvA orbits inherited from the same Fermi surface span the whole range of the angle as shown in Fig. 16. The dHvA frequencies are lowest around [111] orientation (angle= 54.7356^o) and the value is around 1.5 kT. The effective band mass is around $5m_e$ where m_e is the free electron mass. For band-3, in Fig. 14, the dHvA frequencies around 2.3 kT spanned through a limited range of angles around [111] as can be understood by the shape of the corresponding Fermi surface. The dHvA frequencies have a local maxima around [111] orientation instead. The effective mass is above $10m_e$. Even though we have a good agreement with the experiment on the dHvA frequencies with a limited angle span, the predicted dHvA frequencies have a local maxima instead of a minimum as observed experimentally. There is uncertainty in assuming magnetization orien-

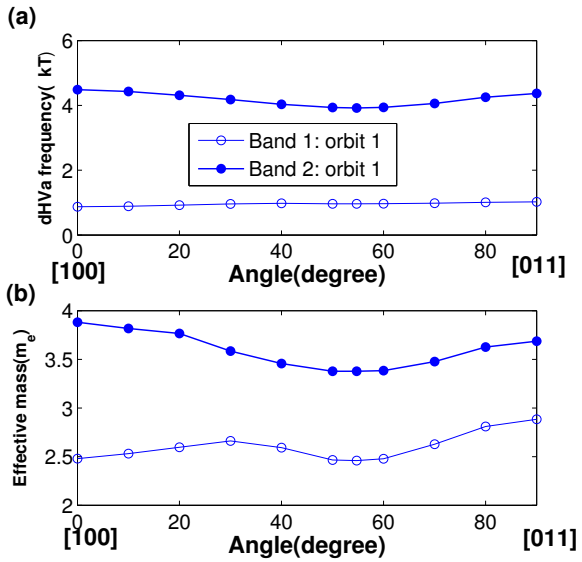

FIG. 11: (Color online) Angular dependence of dHvA frequencies and the average effective mass of the yellow orbits in PM-$PuIn_3$ compound. θ is the angle spanned from the [100] to [011] orientation at the same plane.

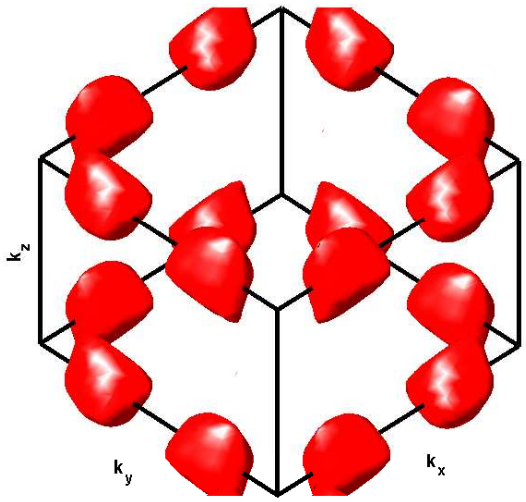

FIG. 12: (Color online) Fermi surface from Band-1 in AFM-$PuIn_3$ compounds with the local spin polarization $\boldsymbol{\sigma} \parallel [001]$.

tation of AFM order along [001] orientation. We expect the orientation of the magnetic order will lead to qualitative effects on the Fermi surface topology because of the strong spin-orbital coupling effects in $PuIn_3$ compounds.

Therefore, we have also considered an easy axis of magnetization along [111] direction. In this case, we predict three $5f$ bands across the Fermi level in this case. We show the Fermi surface topology corresponding to three bands across Fermi level in Figs. 17–19. The details of the dHvA orbits along [111] orientation are shown in Tables VII, VIII, and IX. We identify an orbit with dHvA frequency $F = 2.125$ kT marked by a yellow trace in the Fermi surface around Γ point from Band-2 in Fig. 18. By the calculated angular dependence of the dHvA orbits for Band-2 in Fig. 20(a), we identify the dHvA orbits are limited to certain angle range around [111] orientation. In addition, the effective mass has a local minima around [111] orientation as suggested by experiment.[9] However, the effective mass is only about $2m_e$. For the dual nature of the $5f$ electrons, the temporal quantum fluctuations can renormalize the effective band mass dramatically. We do not expect density-functional theory as presented in this paper can capture this effect. However, the Fermi surface topology and thus the predicted dHvA frequencies should still be robust by Landau's Fermi liquid theories.

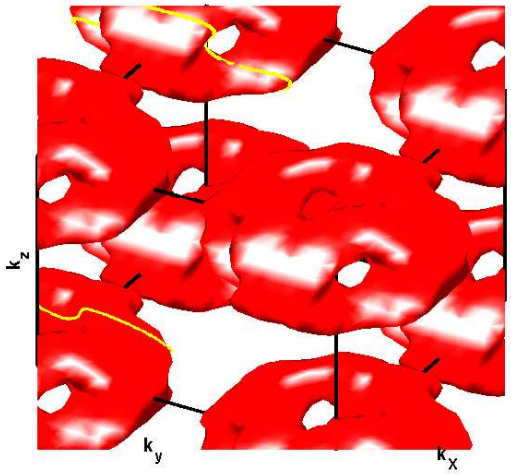

FIG. 13: (Color online) Fermi surface from Band-2 in AFM-$PuIn_3$ compounds with the local spin polarization $\boldsymbol{\sigma} \parallel [001]$.

PM-$PuSn_3$ compound

So far, dHvA effects have not yet been successfully observed in $PuSn_3$ compounds. By our calculation, we find multiple dHvA orbits in a narrow range of frequencies at

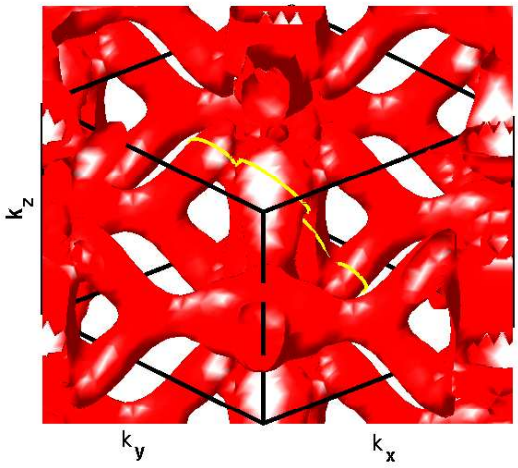

FIG. 14: (Color online) Fermi surface from Band-3 in AFM-$PuIn_3$ compounds with the local spin polarization $\boldsymbol{\sigma}$ ∥ [001].

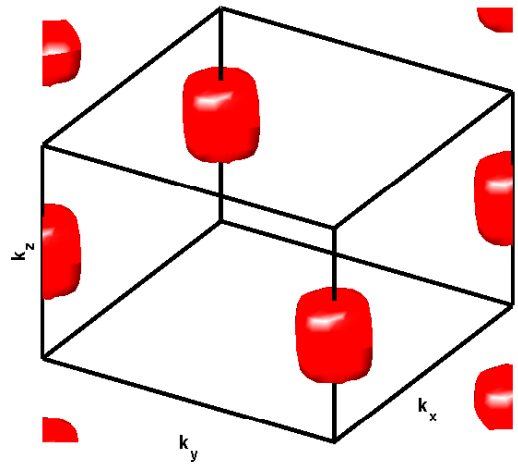

FIG. 15: (Color online) Fermi surface from Band-4 in AFM-$PuIn_3$ compounds with the local spin polarization $\boldsymbol{\sigma}$ ∥ [001].

TABLE III: The dHvA orbit from Band-1: AFM-$PuIn_3$, **B** ∥ [111], $\boldsymbol{\sigma}$ ∥ [001]

F (kT)	$m^*(m_e)$	Type	Number of orbits
0.4424	2.1654	h	2
0.4412	2.3620	h	2

TABLE IV: dHvA orbits from Band-2: AFM-$PuIn_3$, **B** ∥ [111], $\boldsymbol{\sigma}$ ∥ [001]

F (kT)	$m^*(m_e)$	Type	Number of orbits	Color	Label
1.3908	6.2948	h	2	yellow	1
1.006	3.7899	h	2	–	–
0.5189	2.6069	h	2	–	–
0.3335	2.2621	h	4	–	–

TABLE V: dHvA orbits from Band-3: AFM-$PuIn_3$, **B** ∥ [111], $\boldsymbol{\sigma}$ ∥ [001]

F (kT)	$m^*(m_e)$	Type	Number	Color	Label
2.3615	13.4852	e	1	yellow	1
0.7796	1.8097	e	2	–	–
0.6833	3.0840	e	2	–	–
0.577	11.017	e	2	–	–
0.2279	2.2562	e	4	–	–
0.0386	0.8525	e	2	–	–

TABLE VI: The dHvA orbit from Band-4: AFM-$PuIn_3$, **B** ∥ [111], $\boldsymbol{\sigma}$ ∥ [001]

F (kT)	$m^*(m_e)$	Type	Number
0.5277	1.0592	e	1

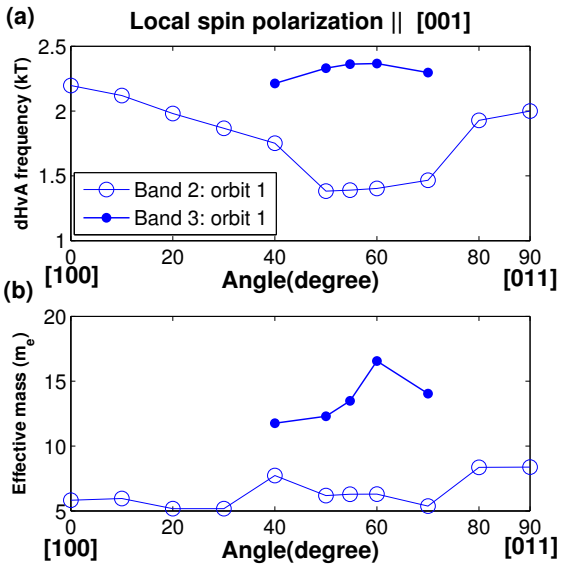

FIG. 16: (Color online) Angular dependence of dHvA frequencies and effective mass of chosen yellow orbits for AFM-$PuIn_3$ compound.

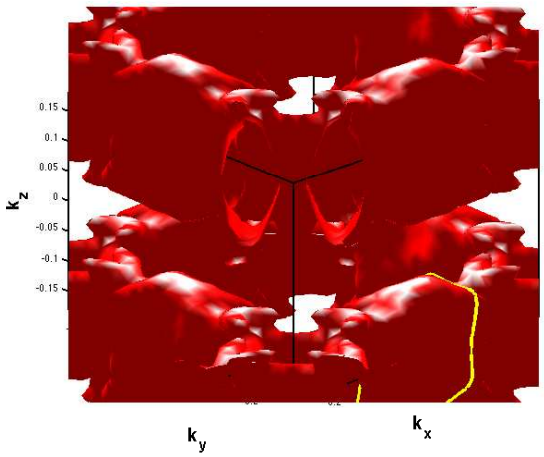

FIG. 17: (Color online) Fermi surface from Band-1 in AFM-$PuIn_3$ compounds with the spin polarization $\boldsymbol{\sigma} \parallel [111]$.

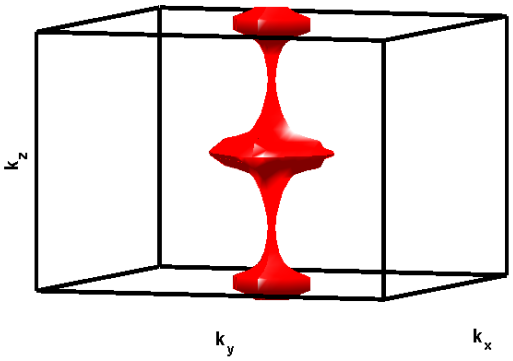

FIG. 19: (Color online) Fermi surface from Band-3 in AFM-$PuIn_3$ compounds with the spin polarization $\boldsymbol{\sigma} \parallel [111]$.

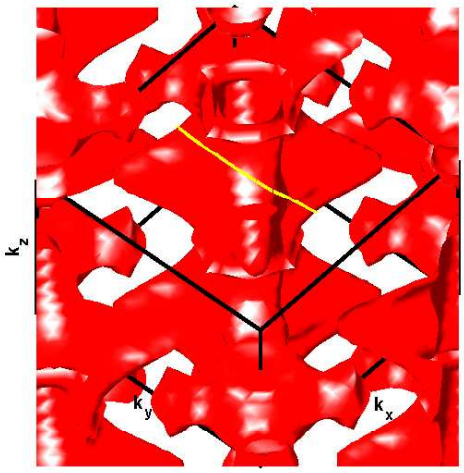

FIG. 18: (Color online) Fermi surface from Band-2 in AFM-$PuIn_3$ compounds with the spin polarization $\boldsymbol{\sigma} \parallel [111]$.

TABLE VII: The dHvA orbit from Band-1: AFM-$PuIn_3$, $\mathbf{B} \parallel \boldsymbol{\sigma} \parallel [111]$

F (kT)	$m^*(m_e)$	Type	Number of orbits	Color	Label
3.2569	5.8858	h	1	yellow	1
1.7165	1.9391	h	1	–	–
0.9876	3.4407	h	2	–	–
0.9697	2.8944	h	2	–	–
0.8421	3.5473	h	2	–	–

TABLE VIII: dHvA orbits from Band-2: AFM-$PuIn_3$, $\mathbf{B} \parallel \boldsymbol{\sigma} \parallel [111]$

F (kT)	$m^*(m_e)$	Type	Number of orbits	Color	Label
3.7022	6.2443	e	1	–	–
2.1250	1.9877	e	1	yellow	1
1.2687	2.8742	e	2	–	–
1.1595	1.5520	e	1	–	–
1.0834	1.7674	e	2	–	–

TABLE IX: dHvA orbits from Band-3: AFM-$PuIn_3$, $\mathbf{B} \parallel \boldsymbol{\sigma} \parallel [111]$

F (kT)	$m^*(m_e)$	Type	Number
0.3359	2.3248	e	1
0.3358	2.4819	e	1
0.3056	2.1990	e	1
0.1935	1.7949	e	1

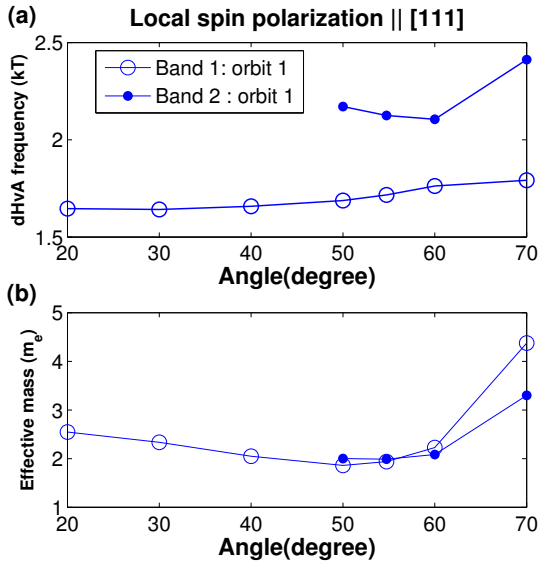

FIG. 20: (Color online) Angular dependence of dHvA frequencies and effective mass of the chosen yellow orbits for AFM-$PuIn_3$ compound.

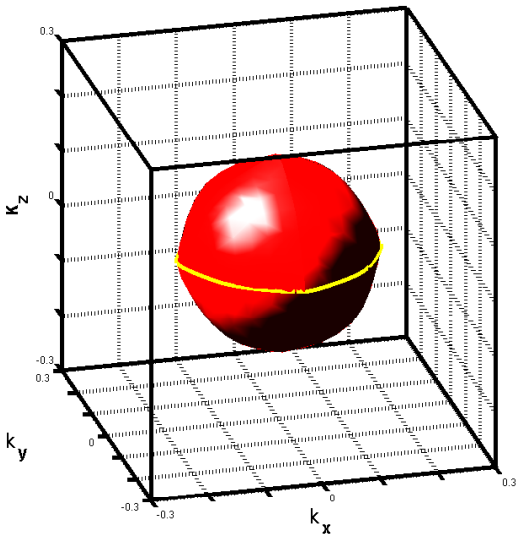

FIG. 21: (Color online) Fermi surface from Band-1 in PM-$PuSn_3$ compound.

TABLE X: The dHvA orbit from Band-1: PM-$PuSn_3$, **B** ∥ [001]

F (kT)	$m^*(m_e)$	Type	Number	Color
3.273	1.5976	h	1	yellow

TABLE XI: dHvA orbits from Band-2: PM-$PuSn_3$, **B** ∥ [001]

F (kT)	$m^*(m_e)$	Type	Number of orbits	Color
0.5550	0.4749	h	2	yellow
0.6873	0.7955	h	4	blue
1.230	1.6842	h	2	green
1.312	0.8721	h	1	white

the field orientation [111]. This may cause complications on observing clean signals. However, we do find a simple Fermi surface topology at the field orientation [001], which can be easier to observe and thus is the case we focus on in this section. With the $PuSn_3$ band structure in Fig. 4, we observe two energy bands crossing the Fermi energy E_F, which only have similar dispersion as PM-$PuIn_3$ near the point $\Gamma = (0, 0, 0)$ in BZ. The cutting points at the Fermi energy in Fig. 4 are the projection of the three dimensional Fermi surface plot along the line between symmetry points in BZ. We show the Fermi surfaces for those two bands in Figs. 21 and 22, respectively. Our calculation shows one hole-like (yellow) orbit (with $F = 3.273$ kT) near the Γ point in the BZ, which agrees with the band dispersion at Band-1 near the Γ point. For Band-2, the four dHvA orbits are identified and all of them are hole-like at the field orientation [001] (See Table VIII), denoted by colored closed curves in Fig. 22. The maximum dHvA frequency is given by the white cyclotron orbit with $F = 1.312$ kT near the M point in BZ. By observing the Fermi points and the band dispersion nearby for Band-2 in Fig. 4, one can see the agreement with the Fermi surface. In addition, from the Fermi surface topology, one can see there is no clear evidence for a dominant Fermi surface nesting. This might explain the absence of magnetism in $PuSn_3$.[13]

In Fig. 23, we show the field angle dependence of dHvA frequencies for the yellow dHvA orbit in Band-1 and the white dHvA orbit in Band-2. The magnetic field varies from the crystal orientation [100] to [001] in the $PuSn_3$ compound. We observe that the dHvA frequencies are symmetrical with respect to the orientation at the angle 45^o. The dHvA frequency for Band-1 is insensitive to the orientation because of the corresponding spherical Fermi surface near the Γ point and is well separated in frequencies from the orbits due to Band-2. However, the Fermi surface circled by the white orbit in Band-2 is not spherical (shown in Fig. 22); therefore, a strong field angle dependence due to the Fermi surface is obtained.

IV. CONCLUSIONS AND DISCUSSIONS

We have studied the electronic properties for compounds $PuSn_3$ and $PuIn_3$ within density functional theory under the GGA approximation. Our calculations for AFM-$PuIn_3$, with magnetization along [001] direction, show that the Fermi surfaces with heavy effective band mass produce the dHvA frequencies near 2 kT, in quan-

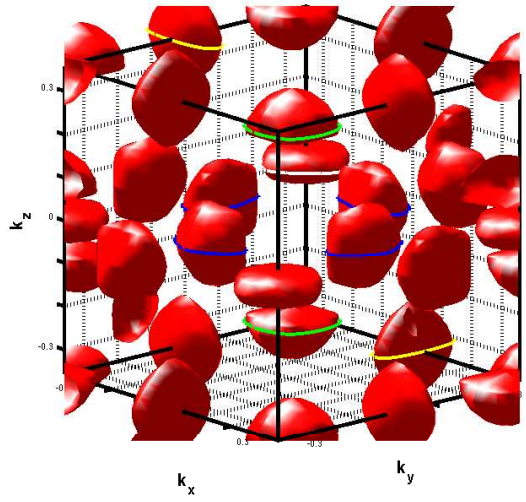

FIG. 22: (Color online) Fermi surface from Band-2 in PM-$PuSn_3$ compound.

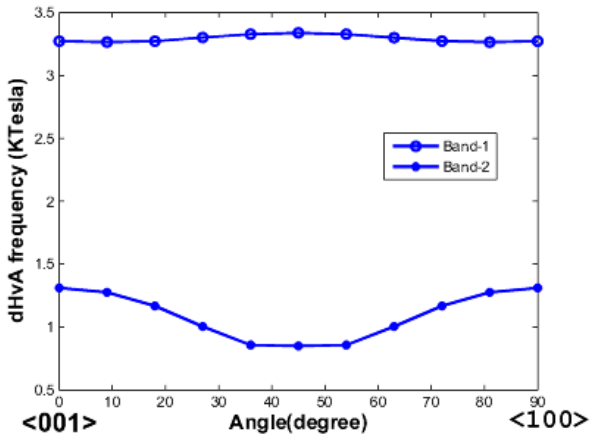

FIG. 23: (Color online) Angular dependence of dHvA frequencies in PM-$PuSn_3$ compound. The dHvA orbit of Band-1 is inherent from the same Fermi surfaces circled by the yellow orbit in Fig. 17. The dHvA orbit of Band-2 at different angle is inherent from the same Fermi surfaces circled by the green orbits in Fig. 18.

titative agreement with experiments but the angular dependence of dHvA frequencies around [111] orientation cannot be reconciled with experiment. However, when the magnetization is parallel along [111] direction, we can identify new orbits showing good agreement with experimental measurement in dHvA frequencies. We point out the predicted effective band mass values can be further renormalized due to temporal quantum fluctuations which cannot be captured properly with the density-functional theory. We suggest experimental investigations of the effective band mass of the dHvA orbits and the magnetic order are crucial to resolves those issues. Finally, we have also predicted the band structure and dHvA frequencies for $PuSn_3$, which is known to be paramagnetic, for guiding the search of dHvA effects in the $PuSn_3$ inter-metallic compounds. Experimental observation of these frequencies in the compound will help the search for quantum oscillations in δ-phase of Pu. We do not expect the predicted values for the effective mass is reliable with density-functional theory ignoring strong quantum temporal fluctuations but the predicted Fermi surface should be robust with respect to the given magnetic order.

Acknowledgments

We thank Eric D. Bauer, Ross D. McDonald, Matthias J. Graf, and P. M. C. Rourke for helpful discussions. This work was supported by U.S. DOE at LANL under Contract No. DE-AC52-06NA25396 and LANL LDRD-DR Program (C.-C.W. & J.-X.Z.)

[1] K. T. Moore and G. van der Laan, Rev. Mod. Phys. **81**, 235 (2009).
[2] A. M. Boring and J. L. Smith, Los Alamos Sci. **26**, 91 (2000).
[3] N.G. Cooper (ed.) *Challenges in Plutonium Science*, Los Alamos Sci. **26** (2000).
[4] J. L. Sarrao, L. A. Morales, J. D. Thompson, B. L. Scott, G. R. Stewart, F. Wastin, J. Rebizant, P. Boulet, E. Colineau and G. H. Lander, Nature **420**, 297 (2002).
[5] F. Wastin, P Boulet, J Rebizant, E Colineau and G H Lander, J. Phys.: Condens. Matter **15**, S2279 (2003).
[6] E. D. Bauer, M. M. Altarawneh, P. H. Tobash, K. Gofryk, O. E. Ayala-Valenzuela, J. N. Mitchell, R. D. McDonald, C. H. Mielke, F. Ronning, J. C. Griveau, E. Colineau, R.

Eloirdi, R. Caciuffo, B. L. Scott, O. Janka, S. M. Kauzlarich, and J. D. Thompson, J. Phys.: Condens. Matter **24**, 052206 (2012).

[7] Jian-Xin Zhu, P.H. Tobash, E. D. Bauer, F. Ronning, B. L. Scott, K. Haule, G. Kotliar, R. C. Albers, and J. M. Wills, Europhys. Lett. **97**, 57001 (2012)

[8] H. Yasuoka et al., unpublished; C. H. Booth, Y. Jiang, D. L. Wang, J. N. Mitchell, P. H. Tobash, E. D. Bauer, M. A. Wall, P. G. Allen, D. Sokaras, D. Nordlund, T.-C. Weng, M. A. Torrez, and J. L. Sarrao, Proc. Natl. Acad. Sci. **26**, 10205 (2012).

[9] Y. Haga, D. Aoki, H. Yamagami, T. D. Matsuda, K. Nakajima, Y. Arai, E. Yamamoto, A. Nakamura, Y. Homma, Y. Shiokawa, and Y. Ōnuki, J. Phys. Soc. Jpn. **74**, 2889 (2005).

[10] H. H. Hill, *The early "actinides": The periodic system's f electron transition metal series, in: Plutonium 1970 and Other Actinides* (Edited by W. N. Miner), p. 2, AIME, New York (1970).

[11] F. H. Ellinger, C. C. Land, and K. A. Johnson, Trans. Metall. Soc. AIME **233**, 1252 (1965).

[12] S. M. Baizaee and A. Pourghazi, Physica B **387**, 287 (2007).

[13] V. Sechovsky' and L. Havela, *Intermetallic Compounds of Actinides*, Vol 4, The Handbook of Ferromagnetic Materials, edited by E. P. Wohlfarth and K. H. J. Buschow (North-Holland, Amsterdam, 1988)

[14] J. P. Perdew, K. Burke, and M. Ernzerhof, Phys. Rev. Lett. **77**, 3865 (1996).

[15] E. Sjostedt, L. Nordstrom, and D. J. Singh, Solid State Commun. **114**, 15 (2000).

[16] P. Blaha, K. Schwarz, G. Madsen, D. Kvasnicka, and J. Luitz, WIEN2K, An Augmented Plane Wave + Local Orbitals Program for Calculating Crystal Properties (K. Schwarz, Tech. Univ. Wien, Austria) (2001).

[17] D. D. Koelling and B. N. Harmon, J. Phys. C **10**, 3107 (1977).

[18] J. Kunes, P. Novak, R. Schmid, P. Blaha, and K. Schwarz, Phys. Rev. B **64**, 153102 (2001).

[19] J. M. Lawrence and S. M. Shapiro, Phys. Rev. B **22**, 4379 (1980).

[20] N. D. Mathur, F. M. Grosche, S. R. Julian, I. R. Walker, D. M. Freye, R.K. W. Haselwimmer, and G. G. Lonzarich, Nature **394**, 39 (1998).

[21] D. Shoenberg, *Magnetic Oscillations in Metals*, Cambridge University Press (1984).

[22] P.M.C. Rourke and S. R. Julian, Comput. Phys. Commun. **183**, 324 (2012).

[23] O. Erickson, M. S. S. Brooks, and B. Johansson, Phys. Rev. B **39**, 13115 (1989).